Recent Trends in Sturctural Integrity Assessment, Eds.: V.R. Ranganath, S. Tarafder, A. Bahadur, 18-19 January 2001, National Metallurgical Laboratory, Jamshedpur, India, pp.85-104.

Assessment of Defects and Microstructures for Evaluating Damage in Pressure Retaining Components

BALDEV RAJ and T. JAYAKUMAR

Indira Gandhi Centre for Atomic Research, Kalpakkam - 603 102.

ABSTRACT

Reliable, safe and economical operation of pressure retaining components in various industrial plants depends on the importance given to quality assurance during fabrication and heat treatment of components and in-service performance assessment. Such an approach helps towards improved productivity, prevents unanticipated down time of plants, catastrophes etc. These objectives are satisfactorily met by adopting appropriate non-destructive testing and evaluation (NDT&E) procedures. We discuss in this paper our experience on development and application of a variety of NDT&E techniques for assessment of defects and microstructures in various pressure retaining components of industrial plants.

INTRODUCTION

Safe and reliable performance of pressure retaining components in various industrial plants is essential to withstand global competition. To meet this requirement through non destructive testing and evaluation (NDT&E), greater emphasis is being given for detection of defects with high sensitivity, complete characterization of defects with respect to their exact size, type and shape, characterization of microstructures and evaluation of residual stresses in engineering materials and components. Improved sensitivity for detection of defects not only enables economic design but also effective life management of engineering components. To meet these demands, many developments are taking place in the area of NDT&E. Many advancements in NDE techniques have become possible because of rapid progresses in various fields such as electronics, computer sciences, instrumentation and robotics. Significant progress has been made in establishing quantitative correlations between the life fraction, the damage and the physical property on which the NDT technique is based.

The choice of the NDE technique depends on many factors including, material, geometry, defect type and location, applicability, accessibility and suitability. It may be sometimes necessary to use a combination of two or more techniques, in the best complementary way, to carry out complete and reliable inspection. In this regard, detailed mock-up studies are essential prior to actual inspection, to optimize equipment parameters, design and selection of sensors, selection of standard defects, operating conditions and procedure for recording and evaluation of NDE data to arrive at the desired sensitivity and reliability. Extensive efforts are being made for enhancing the sensitivity and reliability for defect detection, quantification and characterization of nature of defects,

characterization of microstructural features and evaluation of residual stresses using several improvements in the existing techniques and procedures and innovating many new techniques and methodologies including signal analysis, image processing, artificial intelligence and expert systems. Automation of NDE techniques is being increasingly attempted to enable large area scanning, elimination of human fatigue and uncertainty, avoidance of access constraints for manual inspection, increasing speed, on-line assessment etc.

In this paper, the experience of the authors in development and application of various NDT&E techniques for assessment of defects and microstructures for evaluating damage in pressure retaining components used in various industrial plants is discussed.

DEVELOPMENTS IN EDDY CURRENT TESTING TOWARDS QUANTITATIVE CHARACTERISATION OF DEFECTS

Eddy current imaging

Imaging techniques are playing an important role in non-destructive evaluation. While imaging techniques have been routinely applied for visual, X-ray and ultrasonic applications, eddy current imaging (ECI) is a recently emerging trend in the field of eddy current testing [1]. In this ECT technique, scanning the surface of an object in a raster fashion, measuring impedance point by point and converting these data into gray levels format images. The images represent complete information about the extent of discontinuities in two dimensions. Images of welds, notches, corrosion pits and cracks are generated using this approach for quantitative evaluation. Imaging techniques have the potential for automating the measurement process, providing estimates of defect sizes from the image data and improving the probability of detection. An ECI system has been built around a Personal Computer (PC) at the authors' laboratory to scan the object surface and create impedance changes in a laboratory environment.

Detection of weld centre line in austenitic stainless steel welds

Many a time, it would be necessary to remotely inspect welds by ultrasonic testing. Identification of weld centre line is necessary for fixing the required skip distance and scan ranges for ultrasonic testing. In the case of austenitic stainless steel welds, by making use of the presence of delta ferrite in the material, eddy current inspection can be employed for identification of weld centre line. An example is given here. The precise location of the weld centre line, in the inner vessel of Prototype Fast Breeder Reactor (PFBR), is required as a feedback information for remote operation of robots for detailed inspection of the weld by other NDT techniques. Feasibility studies have been carried out to precisely locate the weld centre line. Butt weld joints of 2mm thick AISI type 316 stainless steel plates were studied to accurately locate the weld centre line. The filtering techniques can be employed if the image data are of reasonable length (i.e. the scanned area is limited). These techniques are generally employed after acquiring the data. However, in the test object envisaged, the surface of the reactor vessel of a few metres in diameter is proposed to be scanned remotely with a crawler fixed with a probe scanner. Thus, continuous data is generated which is enormous. In such a case, employing filtering

techniques may not be simple. Therefore in this study, improved probe design was adopted to get better point spread function and image processing techniques were confined to those that could be implemented on-line/real time. Ferrite cored probe operating at a test frequency of 100kHz. Have been used to get better point spread function giving reasonably resolvable images without filtering.

Due to predominant variations in the electrical conductivity and magnetic permeability (due to the presence of delta ferrite), the weld region has been distinctly noticed in the eddy current images. The change in the impedance has been found to vary from the base metal - weld interface to the weld - base metal interface and thus reaching a peak at the centre of the weld. Thus the precise location of the weld centre line can be found from the eddy current image. The accuracy of detection of the weld centre line is found to be $\pm$0.1mm. The ECI studies have been further extended to develop an Intelligent Imaging Scheme (IIS) for quantitative evaluation of defects and the same is described in the following section.

IIS for automated eddy current testing of austenitic stainless steel plates and welds

A new IIS has been developed for fast and automated eddy current (EC) non-destructive testing of austenitic stainless steel (SS) plates and welds [2]. This scheme quickly detects defects in the presence of disturbing variables such as surface roughness, material property/microstructural variations, lift-off, edge-effects etc., and produces accurate three-dimensional pictures of the defects. This is accomplished through the synergistic use of artificial neural networks and image processing methods. In order to realise on-line detection and accurate depth evaluation of defects in the presence of the disturbing variables, a three-layer feed forward error back-propagation neural network with 12 input nodes (EC time-domain parameters from two frequencies), 5 hidden nodes, and 1 output node (defect depth in mm) has been developed. This performance has been realised through the utilisation of the increasing semi-linear portion of the sigmoidal transfer function and by incorporating a 4^{th} order polynomial fit between the computed depths and the actual depths. After systematic training with calibration defects and disturbing variables, this network has been used in conjunction with raster-scan imaging and data acquisition system to produce accurate depth-profile images. Since the depth-profile images are blurred, for their restoration a new image processing approach that uses morphological thinning has been developed. The EC probe for imaging has been optimised using an indigenously developed finite element model. The intelligent imaging scheme as illustrated in Fig. 1 involves the following steps:

- imaging of pre-defined region at a coarse scan interval (ΔS) using a neural network trained with linear and circular defects for mere defect detection purpose,
- automatic identification of boundaries of all defects using an image processing method called chain-code,
- identification of defect shape using the aspect ratio (> 2 linear, < 2 circular),
- imaging only the defective regions at a fine scan interval using separate neural networks for accurate depth quantification of linear and circular defects,

- applying the image processing approach to the fine-scan depth-profile images for accurate restoration of length, width and orientation of the defects,
- fusion of the depth-profile and restored images to form a comprehensive 3-dimensional picture of the defects and tabulation of defects in the imaged region.

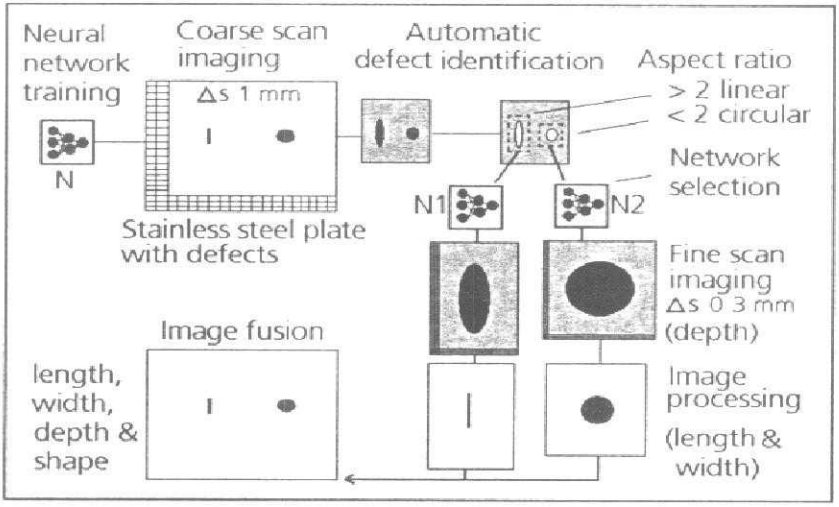

Fig. 1: The intelligent imaging scheme developed for quick and automated eddy current testing.

Typical results of application of the scheme to a stainless steel plate consisting of a notch (length 3mm, width 0.3mm and depth 0.8mm) and a flat-bottomed hole (diameter 1.5mm and depth 0.5mm) are shown in Fig. 2. Since the aspect ratio of the notch and hole are different, separate neural networks have automatically been chosen by the scheme for their use during the fine-scan imaging. The imaging scheme has also been successfully applied to austenitic stainless steel welds for automatic detection and evaluation of defects in the presence of microstructural variations, δ-ferrite, surface roughness and edge effect. Application of this scheme to SS plates and welds has resulted in a high probability of detection and a ten-fold reduction in the imaging time, besides ensuring accurate three-dimensional reconstruction of defects. Further, the on-line neural network method has been applied for on-line testing of indigenously produced FBTR cladding tubes (diameter 5.1mm, thickness 0.38mm) with periodic thickness variations (~ $\pm$20 microns) that disturb testing. Through holes of diameter larger than 200 microns have been successfully detected.

Pattern recognition approach to defect detection and characterisation by eddy current testing

Eddy current testing is one of the widely used Nondestructive Evaluation (NDE) techniques for inspection of surface and sub-surface defects in electrically conductive materials. This methodology is dependent on the generation and use of a calibration curve correlating one or more of the signal parameters like amplitude/phase with the size of standard reference defects such as holes and notches. These calibration curves are

however inherently limited by the use of reference defects of fixed shapes. Besides the amplitude and the phase, a defect signal in the impedance plane is considered to carry information in its pattern about the defect shape. The uncertain role of many factors (including defect shape and orientation) on calibration curves has limited the conventional analyses in achieving improved reliability in defect detection and characterization.

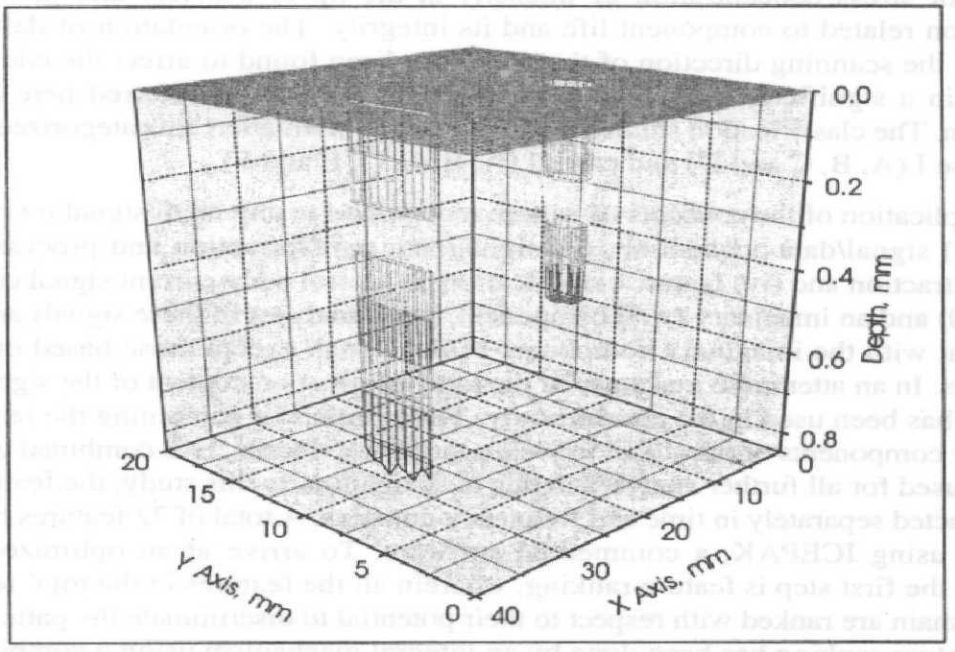

Fig. 2: Results of the intelligent imaging scheme showing the three-dimensional picture of a defective region in an austenitic stainless steel plate with two defects.

The material chosen for this study is AISI type 316 stainless steel with generated defects of two types (a) artificial, and (b) natural ones. Artificial defects were of two types, viz. holes and rectangular notches, and were of varied sizes and configurations in terms of partial and through thickness type. The generated natural defects were of three types, viz. fatigue cracks, stress corrosion cracks and wall thinning defects.

Characterizations of the artificial and the natural defects in the specimens were carried out by placing these on a rigid platform and scanning the eddy current probe in the regions of interest. These tests were performed with the help of a multifrequency system. The scanning patterns have been designated as A, B, C, D, E, F, G and R, for convenience of subsequent discussion. The eddy current analogue signals were digitized and acquired using a 12-bit signal analyzer using a sampling frequency of 500Hz and a data length of 2K (2048 points). Different categories of the eddy current records, were: (i) no-flaw, (ii) hole, (iii) notch, (iv) fatigue cracks and (v) stress corrosion cracks.

The reliability in detection of defects obtained by conventional analyses of Eddy Current Signals (ECS) has always been a topic of study because, interpretation of a visual output depends on human operators. In this study the performance of each ANN to

correctly classify a signal as originating from a defect or no-defect area has been assessed [3]. The defect type essentially implies the morphology or shape of a defect in two dimensions i.e., whether it is rounded (pores, voids, inclusions, pits, etc.) or rectangular/obloid (cracks, etc.). The classification of the defect shape is an important aspect for analysis of ECS because it provides the indication of the severity of the defect in terms of stress concentration or intensity at the tip of a defect and in turn gives information related to component life and its integrity. The orientation of defects with respect to the scanning direction of the probe has been found to affect the eddy current behavior in a significant way. This aspect for convenience is referred here as defect orientation. The classification studies related to defect orientation are categorized into two parts: Case I (A, B, C and D) and case II (A, B, C, D, E and F).

The application of the concepts of pattern recognition to any NDE signal involves four phases: (i) signal/data acquisition, (ii) signal/data transformation and processing, (iii) feature extraction and (iv) feature classification. A typical eddy current signal consists of a real ($x(t)$) and an imaginary ($y(t)$) component. Most analyses of these signals are usually carried out with the imaginary component of the signal, except those based on Fourier descriptors. In an attempt to make use of the total information content of the signal, a new approach has been used in the current study. This consists of combining the real and the imaginary components of the signal to yield a single waveform. This combined waveform has been used for all further analyses in this investigation. In this study, the features have been extracted separately in time and frequency domains. A total of 72 features have been extracted using ICEPAK, a commercial software. To arrive at an optimized feature selection, the first step is feature ranking, wherein all the features in the total feature set of one domain are ranked with respect to their potential to discriminate the patterns under study. Feature ranking has been done by an integral mechanism using a combination of the inter- and intra-class distances and the use of the Fisher approach. Once the features were ranked for a specific classification problem, further analyses with respect to defect detection and characterisation were carried out using a Multi - Layered Perceptron (MLP) based artificial neural network. The index of performance of a classifier was evaluated on the basis of its capability to achieve optimum classification.

The pattern recognition analysis was carried out using an ANN based on the MLP model. The study demonstrated the excellent performance of the MLP for detection of the artificial (100%) and the natural defects (98%) irrespective of the domain from which the features have been extracted. The optimized architecture for defect detection was found to be 8-8-2 (I-H-O). Independent feature ranking in separate domains and optimization of the MLP are considered as the major governing factors for achieving such better quality of defect detection. The use of frequency domain features have led to better performance of the MLP for the case of defect type (shape) classification. The best observed correct classifications were 98% for the artificial and 100% for the natural defects when the number of features considered ranged between eight and ten. The success achieved in classifying branched and unbranched fatigue and stress corrosion cracks was also excellent with 100% correct classification. The studies resulted in successful classification of 90% and 95% for artificial and natural defects respectively when the frequency domain

features were used as input to the MLP. Correct classifications of 79% and 63% were obtained for case I and case II respectively of defect orientation. The major conclusions of the study were:

i. For MLP, the optimum number of features which resulted in the highest correct classification ranged from six to ten for almost all cases of defect detection and characterization. The optimized set of features varied in type and domain depending on the classification problem.
ii. Use of neural networks trained on artificial defects to evaluate natural defects have demonstrated excellent performances for defect characterization. Perfect (100%) classification of the branched/unbranched nature of cracks can be done using MLP.
iii. The optimized architectures of MLP for the various classification tasks varied with respect to the number of nodes in the input and hidden layers, indicating different levels of complexities in the decision surface separating the different classes.

These, internationally first of its kind, studies discussed above for three dimensional imaging of defects and their quantitative characterization of defects by advanced neural network approaches can be successfully adapted for on-line evaluation of defects based on fracture mechanics approaches.

EDDY CURRENT TESTING FOR INSPECTION OF FERROMAGNETIC PIPES AND TUBES USED IN HEAT EXCHANGERS AND STEAM GENERATORS

While inspection of pressure tubes made of non-ferromagnetic materials by eddy current testing (ECT) is easy, ECT of ferromagnetic tubes used in heat exchangers is difficult due to their high and continuously varying magnetic permeability. These variations produce high amplitude ECT signals that mask the signals from defects. The use of magnetic saturation can overcome these difficulties to a large extent, i.e., the ferromagnetic tubes can be satisfactorily inspected by ECT if they are magnetically saturated. In this area, authors' laboratory has successfully designed high strength Nd-Fe-B permanent magnet based eddy current probe and results were evaluated using a calibration tube with artificial defects [4]. For pre-service and in-service inspection of ferromagnetic tubes, a new technique that is showing great promise and potential is Remote Field Eddy Current Testing (RFECT) is developed. The primary advantages of this technique are (I) the ability to inspect tubular products with equal sensitivity to both internal and external metal loss or other anomalies, (ii) linear relationship between wall thickness and the measured phase lag and (iii) absence of lift-off problems. The technique features the ability to inspect both ferro and non-ferromagnetic materials with equal sensitivity to internal or external anomalies. Pioneering work has been carried out at the authors' laboratory with respect to the development of RFECT instrument and the computer simulation of the technique. Wall loss down to 15 % was detected using an indigenously developed RFECT instrument. The presence of transition and remote field zone and the affect of tube diameter and wall thickness on them have been studied using a 2D- FEM code. An eddy current impedance imaging (ECII) system has also been developed for imaging the defects such as corrosion pits, fatigue cracks *etc.*

Eddy current inspection of steam generator tubes

Many steam generators consist of tubes manufactured from Cr-Mo ferritic steels. These tubes are required to be inspected by both ultrasonic and eddy current techniques as part of the stringent quality control. As discussed earlier, in view of the ferritic nature of the tubes, eddy current inspection is extremely difficult due to the inherent magnetic permeability variations and need the use of special D.C. saturation coils. A special D.C. coil assembly along with eddy current probe was designed and fabricated to achieve the desired saturation level for reliable inspection. The outcome of the results indicated that eddy current inspection is complimentary to ultrasonic techniques for detection of different types of defect such as axial, circumferential, near surface and interior defects. Figs. 3(a, b) show the eddy current signals obtained from good region and from a natural defect respectively.

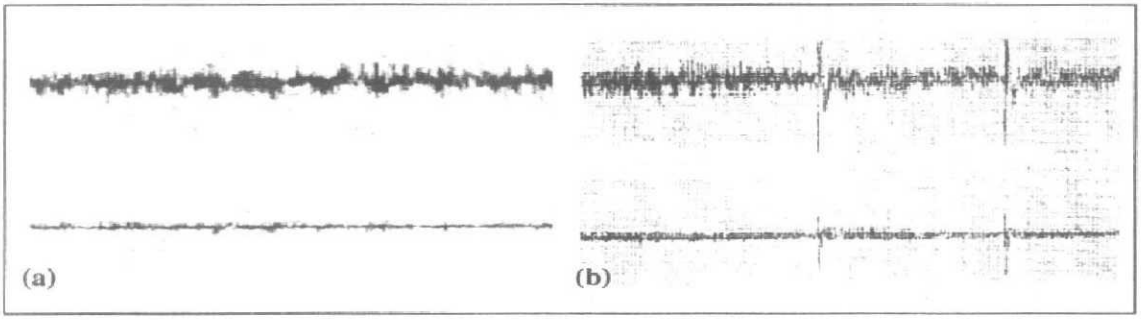

Fig. 3: Eddy current signal from (a) good tube and (b) a natural defect

INSPECTION OF HEAT EXCHANGER TUBES USING INTERNAL ROTARY INSPECTION SYSTEM

Industries like petrochemicals, fertiliser, power etc. are equipped with various heat exchangers and steam condensers for effective heat transfer and also as part of process requirement. As indicated above, NDE and condition monitoring of these heat exchanger/steam condenser tubes are generally carried out by single or multifrequency ECT. However, ECT is not sensitive enough for detection of localised pitting (corrosion) type of defects which are isolated and also defects present under support plates. Also, with ECT the exact circumferential position of the defect can not be identified and only its location along the length of the tube can be identified. Though multi frequency eddy current testing solves this problem of defect detection under baffle plates, evaluation of the defect becomes difficult particularly in the case of carbon steel exchanger tubes because of large variations in the permeability of carbon steel materials. In order to study the feasibility of using internal rotary inspection system (IRIS) to be used as an alternate/complimentary method for multifrequency ECT, studies were conducted on heat exchanger tubes having baffle plates with uniform gap between the tubes and the plate, and tubes where baffle plate makes a contact on the OD of the tube at some points, and tubes having defects at the point on the tube where baffle plate makes a contact [5]. Fig. 4(a) shows the rotating probe head of with a mirror to permit ultrasonic beam to incident

normal to the tube axis. The studies made with IRIS studies indicated that whenever there exists an uniform gap between baffle plate and the tube, the presence of baffle plate is not at all seen in the B-scan picture and only the cross section of the tube is seen. Whenever the tube comes into contact with the plate by way of sagging/swelling, the cross sectional image of the tube and the place of contact of the baffle plate are seen clearly (Fig. 4(b)). It is evident from Fig. 4(c) that the presence of non-contact baffle plate is seen by IRIS due to through and through nature of the defect in the tube wall. In this case, the shift in the baffle plate signal from the tube wall can very well be correlated to the gap between the baffle plate and the tube.

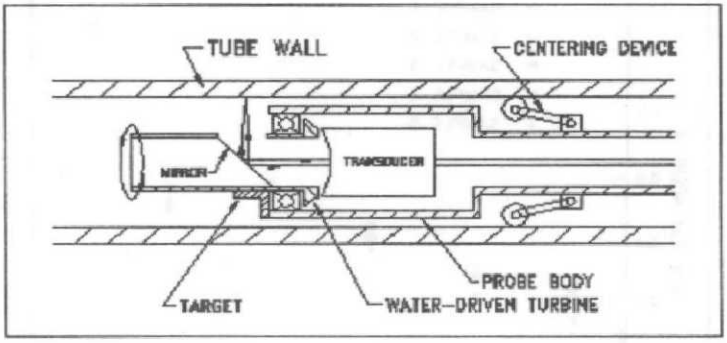

Fig.4(a): Cross sectional view of inspection head of IRIS

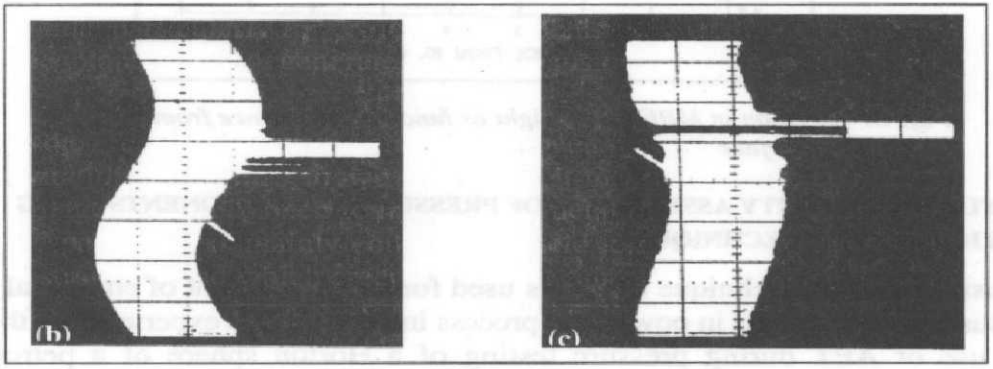

Fig. 4(b): CRT pattern from the Baffle plate at contact region and (c) CRT pattern from a through and through defect under baffle plate.

DETERMINATION OF CASE DEPTH IN CARBURISED COMPONENTS

The feasibility of using magnetic Barkhausen emission (MBE) technique for evaluation of carburization depth in ferritic steel tubes used in a petrochemical industry has been studied [6]. MBE measurements were carried out on samples from service exposed 0.5Cr-0.5Mo ferritic steel tubes at different depths (cross section) from the carburized ID surface, to simulate the variation in carbon concentration gradient within the case depth of MBE with increasing time of exposure of the tubes to carburization. Fig. 5 shows the variation in MBE level with the depth of measurement. It has been observed that the MBE

level increases with increasing depth of measurement. An inverse relation between MBE level and carbon content/hardness value has been observed. This study suggests that the MBE measurements on the carburised surface can be correlated with the concentration gradient within the case depth of the MBE which would help in predicting the appropriate depth of the carburized layer with proper prior calibration. The depth of carburized layer is a deciding factor for continued use of these tubes.

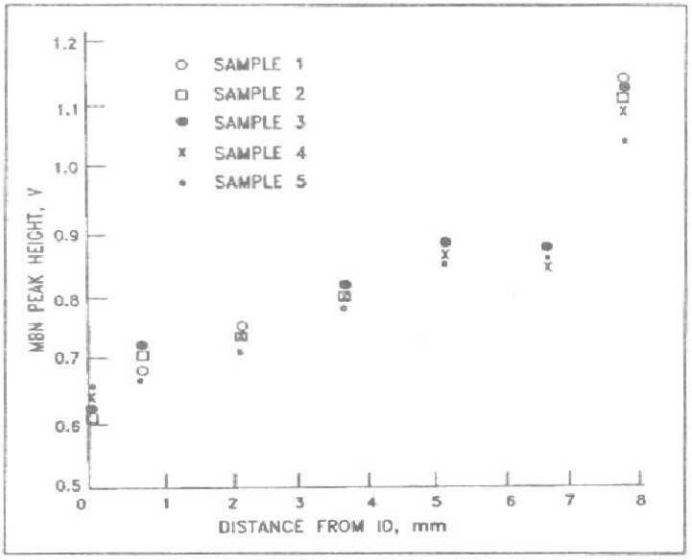

Fig. 5: Variation in MBE peak height as function of distance from inside (ID) surface

STRUCTURAL INTEGRITY ASSESSMENT OF PRESSURISED COMPONENTS USING ACOUSTIC EMISSION TECHNIQUE

Acoustic emission technique (AET) is used for the assessment of structural integrity of pressurised components in power and process industries. The experience of the authors on the use of AET during pressure testing of a Horton sphere of a petrochemical organisation and on-line AE monitoring during operation of a carbon dioxide absorber vessel of a fertilizer plant is discussed.

Hydro testing of a Horton sphere

For AE monitoring during hydro testing of the 17m dia. Horton sphere, a total of twenty four sensors were used in four different groups and in four different configurations to cover the whole structure [7]. In group I, 12 sensors of 150kHz resonant frequency were used in 1-5-5-1 configuration to cover the whole sphere in a triangular location mode (Fig. 6(a)). In group II, three sensors of same frequency were mounted in a triangular location mode to cover a specific region where an indication was observed from the ultrasonic testing carried out earlier. In group III, one broadband (100kHz to 2MHz) sensor was mounted near the suspected region to characterise the deformation and crack

growth signals generated, if any during hydro test. In group IV, eight sensors of 150kHz resonant frequency each were placed in 1-3-3-1 configuration to cover one half of the vessel including the suspected region. The group IV sensors have been connected to a different AE system and used as a backup in case of malfunction of the system used for the group I, II and III sensors. In group I and IV, one sensor each was placed at the bottom and top of the vessel. Based on the response of the sensors to simulated pencil break source, the inter-sensor distance of 9.5m was optimized. Group I, II and III sensors were connected to the sixteen channel Spartan 2000 acoustic emission testing system. Group IV sensors were connected to the eight channel Spartan AT system. By this, the entire vessel could be covered to detect and locate any AE source associated with local plastic deformation and/or growing discontinuities from any part of the sphere.

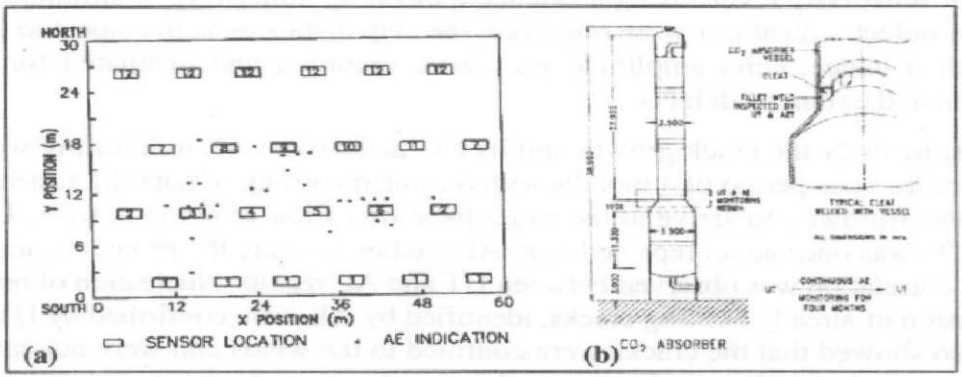

Fig. 6: On-line structural integrity assessment of (a) Horton sphere and (b) Carbon dioxide absorber vessel by acoustic emission technique.

The hydro test of the vessel was carried out to a pressure of 22 x 10^3N/m^2, with periodic holds at different pressures. A reloading cycle from 20 x 10^3N/m^2 to 22 x 10^3N/m^2 was immediately carried out following the first cycle of hydro test. During the hydro test, it was observed that acoustic emission signals were generated only during the pressure rise. With increase in pressure, AE signals were generated only in the newer areas and the areas where AE occurred in the previous pressure steps, do not generate AE in the subsequent pressure steps. These signals were attributed to local micro-plastic deformation of the material. A few signals have also been generated from specific regions, particularly through the entire circumference at an elevation corresponding to the concrete supports. Subsequent inspection of the vessel and simulation pencil break study after the hydro test indicated that the AE signals were generated from the cracks in the concrete columns which were supporting the vessel. Some of the signals could also be confirmed to be due to fracture of oxide scale or paint layer. The results obtained from the broadband sensor were analysed in terms of the spectral energy in different frequency bands. The overall spectral energy was found to increase with pressure rise and this increase was predominantly concentrated in the low frequency band upto 200kHz. This was attributed to the micro-yielding taking place in the sphere. This was also confirmed from the fact

that, during the repressurisation stage (20-22 x $10^3 N/m^2$), the energy of the signals was at the background level, and is attributed to Kaiser effect.

On-line AE monitoring during operation of a carbon dioxide absorber vessel

A carbon dioxide absorber vessel (shown in Fig. 6(b)), in an ammonia plant of a fertilizer plant, made of low carbon steel (39 meters high and maximum diameter of 3.5 meters) had shown signs of deterioration (formation of cracks) in its conical portion during visual, liquid penetrant and magnetic particle inspection. However, it was not possible to decide whether these cracks were only in the fillet welds of cleats or penetrating into the shell thickness (unacceptable from safety point of view). Ultrasonic normal beam and angle beam (45 and 60°.) examinations were carried out after setting the equipment sensitivity levels using a full scale mock up consisting of simulated defects. Whenever defect indications were observed, the skip distances with respect to the probe, beam path distance, echo amplitude etc., were recorded and evaluated for location, orientation and extent of defects.

In order to study the crack growth and its characteristics, AE monitoring was carried out for a continuous period of 4 months with on-line recording of data [8]. Linear location method was followed to arrive at the exact location of the growing defects. Ultrasonic testing (UT) was once again repeated after AE studies to study the growth characteristics. Excellent correlation was observed between UT and AE results. Nucleation of new defects and extension of already existing cracks, identified by AE were confirmed by UT. The UT results also showed that the cracks were confined to the welds and were not entering the shell wall, thus, indicating no damage to the absorber vessel.

DAMAGE ASSESSMENT OF THE ROTOR OF A 13-STAGE STEAM TURBINE

The rotor of a 13-stage steam turbine (Fig. 7(a)) to be used for captive power production in a refinery had suffered damage while being handled at a seaport, which led to the knocking-off of the low pressure side-bearing support. As a result, the entire weight (4.5 tonnes) of the rotor was supported by the last stage, which was touching the ground. Fig. 7(b) shows schematically the type of damage ocurred. Visual inspection revealed considerable damage in the last stage and relatively minor damages in some of the other stages. Trueness check revealed that the rotor was still in an acceptable condition and it was then necessary to find out how many of the rivets between the rotor blade and the shroud had been damaged (possiblly having cracks in the root region). It was also required to find out the extent of the damage at the places where damage could be seen visually. The geometrical conditions were unfavourable for conventional ultrasonic testing as well as for other non destructive testings such as radiography, eddy current testing and magnetic particle testing. Therefore an unconventional (dry couplant) ultrasonic method, where the detection is not based on the reflected energy but on the change in the ultrasonic energy inside the material in a global sense, was employed [9]. The important aspect of this dry-couplant ultrasonic testing method is that the relative positions of the two probes being used in tandem technique is not critical. This technique was used in the through transmission mode (Fig. 7(b)) and it was expected in this configuration that a defect free

rivet would give a higher amplitude display and a rivet with defects would give a lower amplitude signal. The beat pattern was adjusted to give a peak amplitude of 80% with respect to the standard having a rivet without a slit. In one of the rotor stages, on four rivets in a shroud having six rivets, a 50-70% drop in the intensity pattern was observed. This drop in the intensity pattern was the result of crushed or sheared rivets and damage that had taken place up to the region of the rivet root. Although by using the visual inspection, damage in the rivet heads and shroud could be detected, the nature and extent of damage towards the rivet root could only be assessed by the dry-couplant ultrasonic testing. No reduction in the intensity pattern was observed on the rivets of other stages, indicating that they were defect free, even though visual inspection had indicated some minor damage in the shrouds.

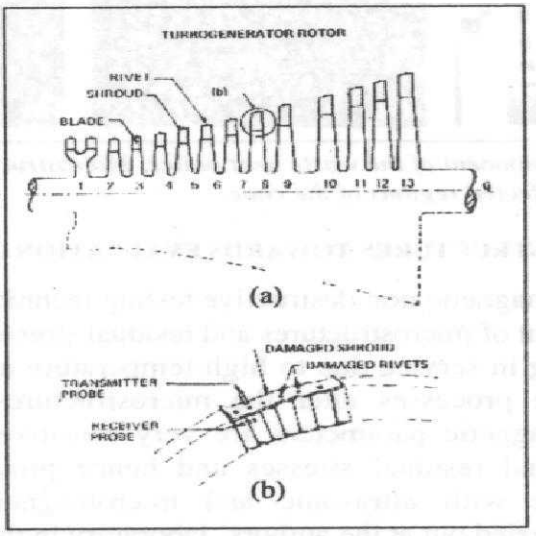

Fig. 7: Schematic sketch showing (a) turbogenerator rotor and (b) damaged shroud/ rivets and ultrasonic probe positions

ASSESSMENT OF IN-SERVICE DEGRADATION OF A CONICAL INLET OF A WASTE HEAT BOILER IN A CHEMICAL PLANT

Many a time, due to malfunction of monitoring devices and deterioration in insulation, plant components operate at higher temperature than permitted. Once such a situation is realized, it becomes mandatory to assess the condition of that component for any degradation and to take a decision on its continued use. A critical assessment has been made by the authors= laboratory to evaluate degradation in a conical inlet of a waste heat boiler in a chemical plant [10]. The conical inlet made of ASTM A 182 Gr F1 (0.5 Mo medium carbon steel), shown in Fig. 8(a), has seen an outside temperature of 623K for a period of six months as against the designed maximum of 393K. The conical inlet carries cracked ammonia at a pressure of 125 x $10^3 N/m^2$ and a temperature of 803K. It is expected that hydrogen damage can take place under these abnormal conditions.

Systematic studies carried out using ultrasonic testing, hardness measurements and in-situ metallography revealed hydrogen damage progressing from the inside surface. The damage was found to be in the form of blisters, pores and micro cracks. Figs. 8(b) and (c) show the microstructure in unaffected (ferrite + perlite) and heat affected region (ferrite + carbides) respectively of the cone. The depth of the damage was quantified using ultrasonic testing. Based on this assessment of the damage, repair of the conical inlet was carried out and reassessed for its further use successfully.

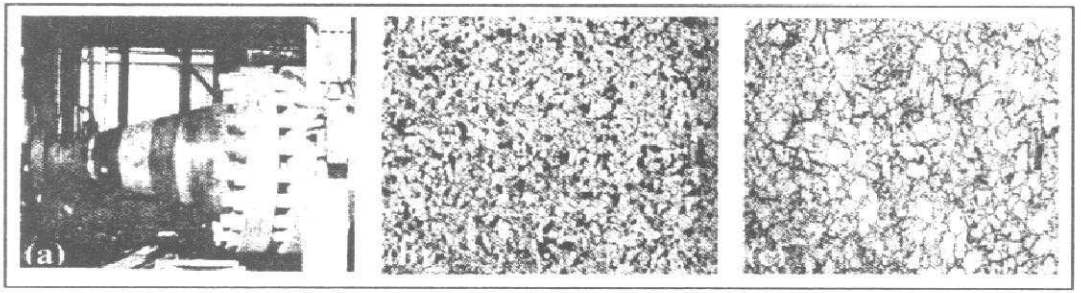

Fig. 8: (a) Conical component of the waste heat boiler; Microstructure of the (b) Unaffected and (c) Heat affected regions of the cone.

ASSESSMENT OF MICROSTRUCTURES TOWARDS EVALUATION OF DAMAGE

Ultrasonic and micromagnetic non destructive testing techniques are being developed and applied for assessment of microstructures and residual stresses to evaluate the damage to components occurring in service due to high temperature ageing, creep and fatigue damage. These damage processes alter the microstructures and residual stresses. Ultrasonic and micromagnetic parameters are very sensitive to microstructural and substructural features and residual stresses and hence provide an opportunity for correlating the damage with ultrasonic and micromagnetic parameters. A few developmental studies carried out at the authors' laboratory in this direction are discussed below.

Assessment of microstructural changes due to thermal ageing in ferritic steels

Magnetic Barkhausen Emission parameters for assessment of grain/lath size and carbide size associated with thermal ageing

During thermal aging of ferritic steel components operating at higher temperatures, the dislocation density, size and distribution of laths/grains and second phase precipitates would vary in a synergistic manner. Micromagnetic and ultrasonic parameters have been identified to characterize these microstructural changes. Using magnetic Barkhausen emission parameters, a two-stage magnetization process has been recently proposed in sufficiently tempered microstructures, considering the grain boundaries and the carbide precipitates as the two major types of obstacle to the domain wall movement. The model has been validated by making studies on the influence of tempered microstructure on the MBE behaviour in carbon steel, 2.25Cr-1Mo steel and 9Cr-1Mo steels [11].

The plot of RMS voltage of the MBE vs. current applied to the electromagnetic yoke systematically changes from a single peak to two peaks with increase in tempering time in carbon steel and Cr-Mo steels as typically shown in Figs. 9(a,b) [11]. Based on the

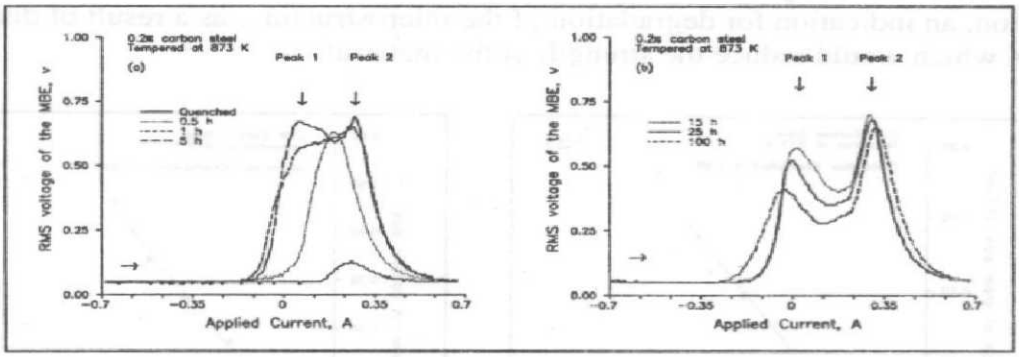

Fig. 9(a-b): Variation in the RMS voltage of the MBE for different tempered 0.2% carbon steel samples

two-stage magnetization process, the MBE peak 1 has been attributed to influence of grain boundaries and the peak 2 to that of carbides [11, 12]. The grain boundaries and precipitates would act as obstacles to the domain wall movement in different field ranges and two peaks in the MBE profile have been observed for these steels in sufficiently tempered condition. The systematic changes in the height and position of these two MBE peaks at different stages of tempering have been explained based on the variations in the lath/grain size and type and size of carbides [11, 12]. Since the formation and growth of reverse domains would become more and more easy with the increase in grain size due to large demagnetizing field at the grain boundaries and hence, the MBE peak 1 position would shift to lower magnetic field as shown in Figs. 9(a, b). Similarly, with increasing tempering time, the carbide size increases. The carbide with higher size offer more resistance to domain wall movement and hence the field corresponding to peak 2 shifts to higher filed, as shown in Figs. 9(a, b). Excellent correlations between positions of MBE peaks 1 and 2 and microstructural parameters (grain/lath size and carbide size), shown in Figs. 10(a, b), indicate that the MBE technique can be used to evaluate the changes in the grain size and precipitate size in long-term aged ferritic steels. However, this is difficult in short-term aged conditions, where the dislocation density is high, and the lath and precipitate sizes are very small.

Ultrasonic velocity measurements for assessment of microstructural changes in 9Cr-1Mo steel

The 9Cr-1Mo steel is used in the normalized (at 1323K for 30 minutes) and tempered (at 1023K for 1 hour) condition. The tempered martensite with fine distribution of M_2X precipitates imparts optimum creep resistance. It was observed that the coherency strain associated with precipitation of needle like M_2X particles along with small amounts of ferrite formation (by dissolution of martensite) up to 1000 hours during aging at 823K and 923K, during initial periods of ageing at 1023K, increases the ultrasonic velocity as shown in Fig. 11 [13]. However, the dissolution of M_2X causes the rapid coarsening of

ferrite grains at longer ageing periods at 1023K and decreases the ultrasonic velocity. Therefore, any increase in velocity with time at a particular location on a component should indicate precipitation of essentially M_2X with very small or no ferrite formation. On the other hand, any decrease in velocity with time would indicate definite ferrite formation, an indication for degradation of the microstructure, as a result of dissolution of M_2X which would reduce the strength of the material.

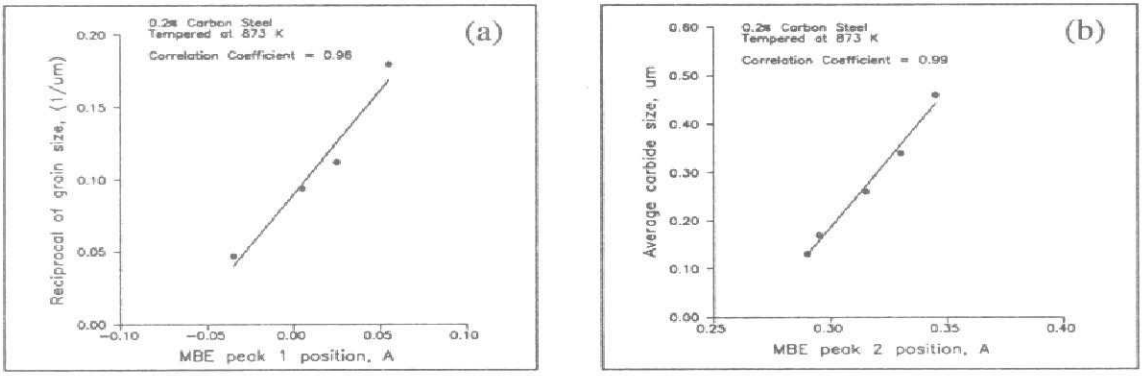

Fig. 10: Relationship between the MBE (a) peak 1 position and average grain size; (b) peak 2 position and the average size of cementite precipitates for various tempered conditions of 0.2% carbon steel.

Ultrasonic velocity for assessment of rejuvenation treatment of service exposed Inconel 625

Nickel based superalloy Inconel 625 has found widespread application in aerospace, nuclear and petrochemical industries due to its excellent combination of corrosion resistance and mechanical properties. Inconel 625 tubes have been used extensively in ammonia cracker units for the manufacture of heavy water. During service, the alloy is exposed to temperatures around 873K for prolonged period, which leads to the decrease in ductility and toughness of the alloy due to heavy precipitation of intermetallic compounds. The degraded mechanical properties of such heavily precipitated components can be regained by giving heat treatments above the service temperature [14].

To study the effect of post service heat treatment, bars of size 10mm x 10mm x 60mm were cut from the service exposed Inconel 625 tube and thermally aged at different temperatures (923K, 1023K and 1123K) for durations up to 500hr. The specimens for tensile testing and ultrasonic measurements were prepared from these bars. The dissolution and precipitation of various phases during post service heat treatments have been studied using ultrasonic velocity measurements [15]. For ultrasonic velocity measurements, the specimens of size 10mm x 10mm x 6mm were prepared from these bars and surface grinding of these specimens was carried out to obtain plane parallelism to an accuracy of better than 3μm. Figure 12 shows the variation of ultrasonic velocity with post service ageing time. In the service exposed condition, ultrasonic velocity has been found to be the highest (5909m/s), because of the heavy precipitation of intermetallic

phases. Heat treatment at 923K, 1023K and 1123K for 1hr decreased the velocity to 5870m/s, 5850m/s and 5830m/s respectively. As the heat treatment temperature increased, more and more precipitates went into solution and hence more decrease in ultrasonic velocity is expected. The ultrasonic velocity has been found to decrease at 1023K up to 10hr and at 1123K up to 1hr only. Beyond this, the precipitation of δ-phase takes place, which leads to a continuous increase in the ultrasonic velocity. Whereas at 923K, ultrasonic velocity has been found to decrease continuously up to 500hr. These variations in ultrasonic velocity have been correlated with the microstructure and mechanical properties such as yield stress and total elongation. Microstructural characterization has been carried out using optical and transmission electron microscopy (TEM). The results revealed that ultrasonic velocity measurements can be used for monitoring the ageing of Inconel 625 during the service and the recovery of mechanical properties by suitable heat treatment can also be ensured by ultrasonic velocity measurements.

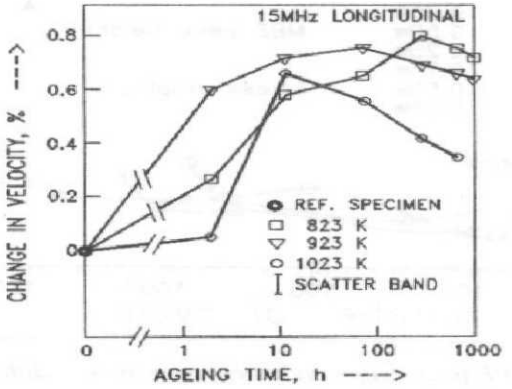

Fig. 11: Variation in the ultrasonic velocity with aging time for 9Cr-1Mo steel.

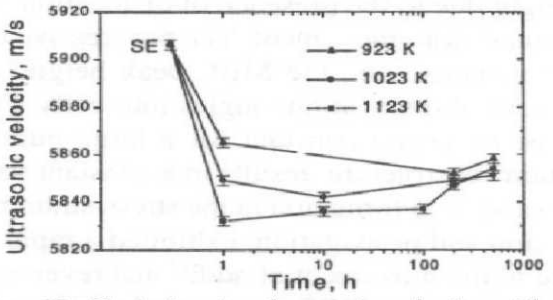

Fig. 12: Variation in ultrasonic velocity with post service ageing time

Fatigue damage in 9Cr-1Mo ferrite steel using MBE technique

Magnetic Barkhausen emission technique has been used to assess the low cycle fatigue (LCF) damage in 9Cr-1Mo ferritic steel. Total strain controlled fatigue tests have been carried out at 300K at strain amplitudes of ±0.25, ±0.50 and ±0.75%. MBE measurements were performed on LCF tested specimens interrupted at various life fractions. The various

stages of deformation and fracture under LCF loading such as cyclic hardening, cyclic softening, saturation and surface crack initiation and propagation have been examined and identified using peak height value of the root mean square (RMS) voltage of the MBE (Fig. 13) [16].

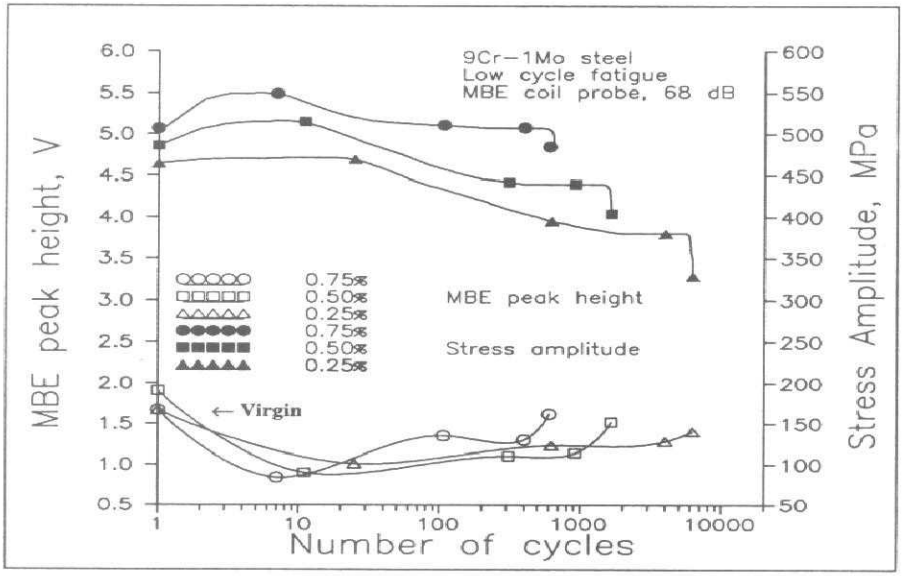

Fig. 13: Variation in the MBE peak height and stress amplitude at different stages of LCF for three different strain amplitudes

The cyclic hardening, which occurs in the early stage of LCF cycling in 9Cr-1Mo steel, decreases the MBE peak height due to the presence of dislocation tangle, which reduces the mean free path of the domain wall movement. The progressive cyclic softening stage displayed reversal in MBE response i.e., the MBE peak height value increased with softening due to rearrangement of dislocation tangles into cells. Further, the saturation stage, where the stress value remained constant for a large number of cycles due to formation of stable dislocation substructure, results in a constant value of MBE. Finally, the onset of rapid stress drop and cusp formation in the stress-strain hysteresis loop, which indicate surface crack initiation and propagation, exhibited a rapid increase in the MBE peak values. This is ascribed to the movement of additional reverse domains produced at the crack surfaces. The rapid increase in MBE due to crack initiation and propagation has been confirmed by the measurement of MBE on the crack and away from the crack using surface MBE probe. This study suggests that the MBE can be used to assess the progressive accumulation of fatigue damage in ferrite steel components.

CONCLUSION

In this paper, the experience of the authors in development and application of a variety of advanced NDE techniques and sensors for assessment of defects and microstructures for evaluating damage in pressure retaining components of various industrial plants has been highlighted.

ACKNOWLEDGEMENTS

We are thankful to a number of colleagues in the Division for PIE and NDT Development of Indira Gandhi Centre for Atomic Research (IGCAR) for their contributions.

REFERENCES

1. B.P.C.Rao, M.T.Shyamsunder, C.Babu Rao and Baldev Raj, Eddy current impedance imaging of surface defects, *Proc. of 7th Asia-Pacific Conf. on NDT*, Shanghai, China, 1993, pp.687-693.
2. B.P.C.Rao, Baldev Raj and M.Kroening, Artificial neural network for on-line eddy current testing, *Review of Progress in QNDE*, **18A**, Eds. D.O.Thompson and D.E.Chimenti, Plenum Press, New York, 1998, pp.813-820.
3. M.T.Shyamsundar, C.Rajagopalan, Baldev Raj, S.K.Dewangan, B.P.C.Rao, and K.K.Ray, Pattern recognition approaches for the detection and characterisation of defects by eddy current testing, Invited for publication in Special Issue on Materials Evaluation, **58**, 2000, pp. 93-101.
4. M.T.Shyamsunder, B.P.C.Rao, C.Babu Rao, D.K.Bhattacharya and Baldev Raj, Partial saturation eddy current inspection of ferromagnetic steam generator tubes, *Proc. National Seminar on NDE (NDE-93)*, Madras, 1993.
5. A.S.Ramesh, C.V.Subramanian, A.Joseph, T.Jayakumar, P.Kalyanasundaram and Baldev Raj, Internal Rotary Inspection System (IRIS)- An useful NDT tool for tubes of heat exchangers, *J. Non-Destructive Evaluation*, **19**, 1999, pp.22-26.
6. V.Moorthy, S.Vaidyanathan, T.Jayakumar and Baldev Raj, Evaluation of carburisation depth in service exposed ferritic steel using magnetic Barkhausen noise measurements, *Materials Evaluation*, 56, 1998, pp.98-106.
7. N.Parida, B.Ravikumar, P.Kumar, D.K.Bhattacharya, T.Jayakumar, C.K.Mukhopadhyay, S.K.Devangan, Baldev Raj, D.C.Patel, S.P.Hariharan and A.Joseph, Acoustic emission testing of LPG Horton sphere, *Proc. Fourth National Workshop on Acoustic Emission (NAWACE-97)*, BARC, Mumbai, 1997.
8. C.V.Subramanian, M.Thavasimuthu, T.Jayakumar, Baldev Raj, C.R.L.Murthy and M.R.Bhat, On-line structural integrity assessment of a carbon dioxide absorber vessel in an ammonia unit of a fertilizer plant, *Proc. National Welding Seminar*, New Delhi, India, 1989. pp.3.1-3.8.

9. M.Thavasimuthu, P.Palanichamy, C.V.Subramanian, D.K.Bhattacharya, Baldev Raj and Jaganath Rao, Inspection of steam turbine rotor blade-to-shroud rivets by dry couplant ultrasonic testing: a case study, *Insight*, **32**, 1990, pp.131-133.
10. M.Thavasimuthu, A.Joseph, A.S.Ramesh, C.V.Subramanian, T.Jayakumar, P.Kalyanasundaram and Baldev Raj, Assessment of in-service degradation of conical inlet of a waste heat boiler in a chemical plant by NDT methods, *Proc. of 14th WCNDT*, New Delhi, 1996, pp.623-626.
11. V.Moorthy, S.Vaidyanathan, T.Jayakumar, Baldev Raj and B.P.Kashyap, *Metall. Mater. Trans. A*, **31**, 2000, pp.1053-1081.
12. B.P.C.Rao, T.Jayakumar, D.K.Bhattacharya and Baldev Raj, *J Pure and Applied Ultrasonics*, **15**, 1993, pp.53-59.
13. V.Moorthy, S.Vaidyanathan, T.Jayakumar and Baldev Raj: *Philosophical Magazine A*, **77**, 1998, pp.1499-1514.
14. Vani Shankar, K.Bhanu Sankara Rao, and S.L.Mannan, Microstructure and mechanical properties of Inconel 625 superalloy, *J. Nuclear Materials*, In Press.
15. Vani Shankar, Anish Kumar, K.Bhanu Sankara Rao, T.Jayakumar and Baldev Raj, *Proc. Int. Symp. on Materials Ageing and Life Management*, Kalpakkam, Oct. 2000, pp.254-260.
16. V.Moorthy, B.K.Choudhary, S.Vaidyanathan, T.Jayakumar, K.Bhanu Sankara Rao and Baldev Raj, *Int. J. of Fatigue*, **21**, 1999, pp.263-269.